

An ideal terrestrial thermometer using carbonate clumped isotopes from gar scales

Katelyn Gray¹ and Mark Brandon²

¹University of Delaware

²Yale University

November 22, 2022

Abstract

Carbonate clumped isotope thermometry has been calibrated for a wide variety of carbonates, including calcite, aragonite, dolomite, siderite, and many of their biogenic forms. The clumped isotope composition of the carbonate group substituting for phosphate or hydroxyl in bioapatite ($\text{Ca}(\text{PO}_4, \text{CO}_3)(\text{OH}, \text{F})$) has also been temperature calibrated using vertebrate tooth enamel from a range of endothermic body temperatures. We apply this method to other bioapatite-bearing taxa and the calibrated temperature range is extended to lower paleoclimatologically relevant temperatures. Furthermore, because relatively large bioapatite samples are required for carbonate clumped isotope measurements ($\Delta 47$), replicate sampling of thin tooth enamel may not be feasible in many situations. Here, we use gar fish (*Lepisosteus* sp.) scales to extend the calibration. These fish are unique in that they are entirely covered in ganoine scales, which are >95% hydroxyapatite. Their enamel structure also makes them resistant to diagenesis. Additionally, gar fossils are common in lacustrine, fluvial, and near-shore facies, and have a wide distribution in time (Cretaceous to modern) and location (North America, South America, Europe, India, and Africa). We have developed a reliable lab protocol for measuring $\Delta 47$ in gar bioapatite. We estimate the standard error (SE) for a single measurement as 0.027 which is based on replicate analyses and Student T-distribution to account for sample size. We report results for modern gar scales from seven North American localities with mean annual water temperatures (MAWT) ranging from 9 to 26 °C. These data give a temperature calibration curve for gar scales of $\Delta 47 = (0.1095 \pm 0.0159) \times 106/T^2 - (0.5941 \pm 0.0548)$ ($R^2 = 0.74$) and a curve for pooled bioapatite of $\Delta 47 = (0.1003 \pm 0.0144) \times 106/T^2 - (0.4873 \pm 0.0495)$ ($R^2 = 0.76$).

1 **An ideal terrestrial thermometer using carbonate clumped isotopes from gar scales**

2 Katelyn Gray^{ab*} and Mark Brandon^a

3 ^a Department of Geology and Geophysics, Yale University, New Haven, CT 06511, United
4 States

5 ^b Department of Plant & Soil Sciences, University of Delaware, Newark, DE 19716, United
6 States

7 * Corresponding author at: 221 Academy St, Newark, DE 19716, United States

8

9 **Keywords:** bioapatite, gar, clumped isotopes, paleotemperature

10 **Declaration of Interest: None**

11

12 **Abstract**

13 Carbonate clumped isotope thermometry has been calibrated for a wide variety of
14 carbonates, including calcite, aragonite, dolomite, siderite, and many of their biogenic forms.
15 The clumped isotope composition of the carbonate group substituting for phosphate or hydroxyl
16 in bioapatite (Ca(PO₄,CO₃)(OH,F)) has also been temperature calibrated using vertebrate tooth
17 enamel from a range of endothermic body temperatures. We apply this method to other
18 bioapatite-bearing taxa and the calibrated temperature range is extended to lower
19 paleoclimatologically relevant temperatures. Furthermore, because relatively large bioapatite
20 samples are required for carbonate clumped isotope measurements (Δ_{47}), replicate sampling of
21 thin tooth enamel may not be feasible in many situations. Here, we use gar fish (*Lepisosteus sp.*)
22 scales to extend the calibration. These fish are unique in that they are entirely covered in ganoine
23 scales, which are >95% hydroxyapatite. Their enamel structure also makes them resistant to

24 diagenesis. Additionally, gar fossils are common in lacustrine, fluvial, and near-shore facies, and
25 have a wide distribution in time (Cretaceous to modern) and location (North America, South
26 America, Europe, India, and Africa). We have developed a reliable lab protocol for measuring
27 Δ_{47} in gar bioapatite. We estimate the standard error (SE) for a single measurement as 0.027%,
28 which is based on replicate analyses and Student T-distribution to account for sample size. We
29 report results for modern gar scales from seven North American localities with mean annual
30 water temperatures (MAWT) ranging from 9 to 26 °C. These data give a temperature calibration
31 curve for gar scales of $\Delta_{47} = (0.1095 \pm 0.0159) \times 10^6/T^2 - (0.5941 \pm 0.0548)$ ($R^2 = 0.74$) and a
32 curve for pooled bioapatite of $\Delta_{47} = (0.1003 \pm 0.0144) \times 10^6/T^2 - (0.4873 \pm 0.0495)$ ($R^2 = 0.76$)
33

34 **1. Introduction**

35 Paleoclimate studies rely heavily on temperature records, and most records come from
36 marine settings; it is relatively difficult to measure past climatical conditions in terrestrial
37 environments. Commonly used methods include leaf shape analysis (Wilf, 1997; Wolfe and
38 Spicer, 1999), the presence and size of ectotherms (Markwick, 1998; Wing and Greenwood,
39 1993), and palynology (e.g., Germeraad et al., 1968; Traverse, 2007). A drawback with leaf
40 shape analysis is a lack of understanding of the underlying physiological basis that defines leaf
41 shape. Historical ectotherm ranges are limited by correlating fossil species with modern analogs.
42 Fossil pollen is highly subject to geologic reworking and may only be resolvable to the family or
43 genus level. Branched GDGTs in soils have been used as a temperature proxy, but the empirical
44 MDT-CBT calibration has large errors of 4.8 °C (1 σ), and may be biased by soil pH and aridity
45 (Peterse et al., 2012). These methods are based on empirical correlations with available climate

46 variables such as surface (as measured at 2 m) air temperature. They are commonly referred to as
47 proxies because they are based on correlations rather than distinct causal processes.

48 Stable isotopic methods provide a more direct approach to measuring paleotemperature.
49 The oxygen isotope method ($\delta^{18}\text{O}$) is the oldest and most widely used, and it has been applied to
50 foraminifera, gastropods, and fish (Grossman and Ku, 1986; Puc at et al., 2010) and carbonate
51 deposits in soils and adjacent lakes (Leng and Marshall, 2004; Swart, 2015). A challenge is that
52 these estimates require an independent measurement of the ambient water at the time of host
53 mineral formation. Carbonate clumped isotopes is a newer method that provides an estimate for
54 both the temperature and the isotopic composition of the water (e.g., Eiler, 2007; Eiler and
55 Schauble, 2004; Wang et al., 2004). Here we apply this method to bioapatite, which is commonly
56 found in teeth, bones, and fish scales.

57 Natural settings have large temperature variations, both in time and space. For example,
58 Still et al. (2019) demonstrate via thermal imaging that temperatures on a hill slope at a point in
59 time range from 35 to 70  C. A long-term record for this hill slope shows that temperatures
60 associated with diurnal and seasonal variations range from 0 to 70  C. This setting has a low
61 potential for producing a useful paleoclimate record, not only because of the large variation in
62 temperature but also because the highly localized temperatures are not connected in a clear
63 manner to regional climate. A counter example is the isotopic record of benthic foraminifera. In
64 fact, the success of this paleoclimate indicator is largely due to the stable and predictable
65 temperature conditions in the deep ocean.

66 We contend that gar scales have the potential to provide a long-term average of surface
67 temperature. They therefore have the potential to provide essential climate information for the
68 terrestrial realm in a manner similar to what benthic foraminifera have done for the deep ocean.

69 Gars have a number of important attributes: (a) they are found in a wide range of terrestrial
70 environments (Lee et al., 1980; Netsch and Witt, 1962) and over a long period of geologic time,
71 (b) individuals have a restricted range and do not migrate (e.g., Buckmeier et al., 2013; Snedden
72 et al., 1999), (c) their scales grow throughout their lifetime, providing a decadal averaged
73 environmental record (e.g., Buckmeier, 2008; Haase, 1969), (d) their scales are highly resistant
74 to diagenesis and commonly occur in the fossil record (Grande, 2010), and (e) the bioapatite in
75 their scales can be analyzed for temperature and isotopic water composition using clumped
76 isotopes.

77 We present a method to prepare and measure gar scale bioapatite for Δ_{47} that is
78 reproducible at a level comparable to analytical error. These Δ_{47} measurements from scales are
79 compared to temperature along a latitudinal gradient in northern North America to calibrate a
80 paleothermometer. ‘Effective temperatures’ are calculated using a method from archaeological
81 dating that takes into account seasonal and diurnal variations in surface air temperatures, which
82 are then adjusted to yearly average riverine and lacustrine temperatures. Lastly, we resolve
83 seasonal growth effects using metabolic rate to estimate effective temperatures, with the
84 potential to be relevant to other paleoclimate studies.

85

86 *1.1. CO₂ clumped-isotope thermometer*

87 The CO₂ clumped-isotope thermometer is based on the concentration of CO₂ molecules
88 with multiply substituted rare isotopes, where ¹³C and ¹⁸O are rare isotopes, and ¹²C and ¹⁶O are
89 common isotopes. The most common doubly-substituted variety of CO₂ is ¹³C¹⁸O¹⁶O, with a
90 mass number of 47. The CO₂ clumped-isotope thermometer compares a sample’s concentration
91 of mass 47 CO₂ to its theoretical concentration if the C and O isotopes were randomly distributed

92 among all mass 47 isotopologues. The ability to accurately measure these isotopologues, which
 93 have concentrations in the parts per million, is a recent technological development. Eiler and
 94 Schauble (2004) applied this method to measure ^{13}C - ^{18}O bond abundance in atmospheric CO_2 .
 95 Ghosh et al. (2006a) showed that CO_2 extracted by phosphoric acid digestion preserved the
 96 isotopologue distribution of the original carbonate anion, CO_3^{2-} , in the host mineral.

97 The Δ_{47} measurement used in CO_2 clumped-isotope measurements is defined in an
 98 idealized fashion by

$$99 \quad \Delta_{47} = [(R^{47}/R^{47*} - 1) - (R^{46}/R^{46*} - 1) - (R^{45}/R^{45*} - 1)]$$

100 where R^{47} , R^{46} , and R^{45} are the abundance ratios of masses 47, 46, and 45 relative to 44, and
 101 R^{47*} , R^{46*} , and R^{45*} are the stochastic values for this ratios (Affek and Eiler, 2006; Eiler, 2007;
 102 Eiler and Schauble, 2004; Wang et al., 2004). In practice, most labs are unable to measure R^{46}
 103 and R^{45} (notable exception is Prokhorov et al. (2019)). Fortunately, variations in R^{47} account for
 104 most of the multiple substitutions that occur in CO_2 (Schauble et al., 2006). As a result, clumped
 105 isotope results are approximated by

$$106 \quad \Delta_{47} \approx (R^{47}/R^{47*} - 1)$$

107 where $R_{46} = R_{46*}$ and $R_{45} = R_{45*}$ (see Appendix A in Zaarur et al., 2013, for details). An
 108 additional approximation involves the isotopic compositions of C and O in the sample CO_2 . $\delta^{13}\text{C}$
 109 and $\delta^{18}\text{O}$ are measured, but the quantity of ^{17}O is not measured directly, and Δ_{47} must be
 110 corrected accordingly for mass interference of ^{17}O . ^{17}O and ^{18}O are related via the relationship
 111 (Brand et al., 2010; Gonfiantini et al., 1995)

$$112 \quad ^{17}\text{R} = \text{K} \cdot (^{18}\text{R})^\lambda$$

113 where K is a coefficient for ^{17}R and ^{18}R in the reference material and λ is a
 114 phenomenological constant that links the fractionation that occurs among the different isotopes

115 of oxygen. By using the λ value of Brand et al. (2010) instead of the original λ value of
116 Gonfiantini et al. (1995), the calculated Δ_{47} was found to be much less sensitive to changes in
117 bulk isotopic composition (Daëron et al., 2016). We use the relevant constant $\lambda = 0.528$ (Brand et
118 al., 2010).

119 The main advantage of carbonate clumped-isotope thermometry is that temperature can
120 be estimated independent of the isotopic composition of the water and dissolved carbon source.
121 Clumped isotopes have been applied to corals (Saenger et al., 2012; Thiagaraian et al., 2011),
122 mollusks (Henkes et al., 2013), brachiopods (Came et al., 2007), and foraminifera and coccoliths
123 (Tripathi et al., 2010). In addition to marine settings, usable carbonates for Δ_{47} can be found in
124 lacustrine settings in the otoliths of fish (Ghosh et al., 2007), terrestrially in the carbonate
125 nodules of fossil soils (Ghosh et al., 2006b), and in the shells of land snails and freshwater
126 gastropods (Zaarur et al., 2011). Carbonate is also found in vertebrate bone, tooth dentin, and
127 enamel, where it occurs in biogenic apatite, primarily in the form of hydroxyapatite,
128 $\text{Ca}_5(\text{PO}_4)_3(\text{OH})$, with carbonate substituting for the phosphate, PO_4^{3-} , and hydroxyl, OH^- , groups.
129 Carbonate clumped isotope thermometry has been calibrated for bioapatite using modern
130 mammalian and crocodylian teeth (Eagle et al., 2010), modern ostrich bone, African elephant
131 enamel, and shark teeth (Löffler et al., 2019; Wacker et al., 2016).

132

133 *1.2 Model species, Lepisosteus spp.*

134 Gars belong to the family *Lepisosteidae* and are ancient Actinopterygians that diverged
135 from crown Teleosts around 342 Ma and have a basal phylogenetic node of 141 Ma (Inoue et al.,
136 2005). They have evolved relatively slowly since this divergence, especially when compared to
137 other vertebrates, including crown Teleosts (Braasch et al., 2016). Today, in North America, gar

138 fish are found in fluvial and lacustrine settings from Canada to Central America and over into the
139 Caribbean. In the geologic record, they were much more widespread, covering every continent
140 except Australia and Antarctica.

141 There are seven different living species in *Lepisoteidae*, all of which are found in North
142 and Central America. We focused on the most common species in North America, *Lepisosteus*
143 *osseus*, which has a distribution that includes drainages in the Mississippi River Valley and the
144 Atlantic margin. When *L. osseus* samples were not available, scales from a sister taxon, *L.*
145 *platostomus*, the shortnose gar, or *L. oculatus*, the spotted gar, were used instead. The tropical
146 gar, *Atractosteus tropicus*, was selected to represent higher temperature tropical environments.
147 All of these species are capable of hybridization and have similar life histories (Bohn et al.,
148 2017). Any phylogenetic, ecological, or other biological effects on scale isotopic compositions
149 are expected to be similar across taxa.

150 A significant amount of body mass and length is accumulated within the first year and
151 growth slows to a steady rate after sexual maturity (Netsch and Witt, 1962). Gar grow year-
152 round (e.g., McGrath, 2010; Solomon, 2012), with faster growth in the first three years of life. At
153 that point, longnose gars have a total length of ~650 mm for males and ~730 mm for females
154 (Johnson and Noltie, 1997). For *L. osseus*, scales do not begin to ossify until a standard snout
155 vent length of approximately 150 mm and bioapatite production begins at 200 mm (Thomson
156 and McCune, 1984). Male longnose gars can live up to 17 years (average 8 years) and females
157 can live up to 25 years (average 9 years) (Smylie et al., 2016). Alligator gar are more long-lived,
158 averaging 11 and 14 years for males and females, respectively (Ferrara, 2001). The upper age
159 limit is >60 years (Buckmeier et al., 2012).

160 An important feature of gar scales for our study is that they grow continuously
161 throughout the gars' adult lives and thus potentially provide a decadal record of surface
162 temperature. The banding in scales is a growth artifact, as it is produced in a manner similar to
163 mammalian enamel (Braasch et al., 2016), which exhibits growth striations on daily and weekly
164 bases (Boyde, 1964; Bromage, 1991; Dean, 1987). The bioapatite is deposited episodically when
165 its base scale reaches a critical size (Thomson and McCune, 1984) and thus scales do not
166 represent seasonal growth cycles.

167 Gar scales have been used in a small number of paleoclimate studies. Fricke et al. (1998)
168 measured $\delta^{18}\text{O}_{\text{phosphate}}$ from fossil gar scales along with mammalian teeth from the Eocene of the
169 Bighorn Basin, Wyoming, USA, to predict $\delta^{18}\text{O}_{\text{water}}$. Fricke and Pearson (2008) measured
170 $\delta^{18}\text{O}_{\text{carbonate}}$ in gar scales from late Maastrichtian fluvial sediments of North Dakota, USA. The
171 temperature of the Late Eocene fluvial sediment in the UK was estimated using a combination of
172 $\delta^{18}\text{O}$ in gar scales, gastropods, otoliths, gyrogonites, and rodent teeth (Grimes et al., 2003). These
173 studies show reproducible measurements and credible temperature estimates.

174

175 **2. Materials and Methods**

176 *2.1 Specimen acquisition*

177 Modern specimens of *Lepisosteus osseus* and *L. platostomus* were acquired either by
178 hook-and-line fishing or through coordination with the Mississippi Wildlife, Fisheries, & Parks
179 Department (Jackson, MS), the Illinois Department of Natural Resources (Springfield, IL), and
180 the Tennessee Wildlife Resources Agency (Nashville, TN), who obtained specimens by gill
181 netting, electrofishing, or collecting by-catch (Table 1 and Figure 1). Where appropriate,
182 individuals were euthanized with an overdose of Tricane methanesulfonate (MS-222), as

183 indicated in Protocol 2012-10681 approved by Yale University's Institutional Animal and Use
184 Committee (IACUC). Specimens were also received on loan from the University of Michigan
185 Museum of Zoology (UMMZ) collections and the Yale Peabody Museum Collections (YPM),
186 either skeletonized or preserved in ethanol. Only specimens with a standard snout vent length
187 >300 mm to a maximum of 774 mm were sampled to ensure a long record of bioapatite growth.

188

189 *2.2 Metabolic Rate and effective temperatures*

190 Most paleothermometers are based on empirically-calibrated proxy relationships. For
191 example, the TEX-86 index is calibrated to the mean annual temperature of the overlying sea
192 surface using Archaea in modern ocean sediment cores. The Archaea that synthesize the GDGT
193 compounds used for the TEX-86 index live throughout the water column, and have the highest
194 abundances below the base of the photic zone (>80 m water depth)(Pearson and Ingalls, 2013).
195 Nonetheless, the design of the calibration means that the TEX-86 temperature equation is
196 optimized to predict mean annual sea-surface temperature, even though Archaea live well below
197 the surface.

198 Isotopic methods are designed, at least in theory, to provide a direct estimate of
199 temperature at the time of precipitation of the host material. More specifically, if one could
200 measure Δ_{47} and calculate temperature at infinitesimal points in a year scale, a large variation
201 would be expected due to variation in ambient temperature throughout the year. The individual
202 Δ_{47} measurements in our study were determined for a full year, which means that they were
203 averaged over multiple years.

204 A key issue is how to relate our Δ_{47} measurements to ambient temperature in a way that
205 avoids the variable temperature associated with diurnal and seasonal variations. To address this

206 issue, we propose using a method that accounts for variable environmental temperature in the
207 racemization of amino acids and hydration of volcanic glass, which are used as dating methods
208 in archeology and geomorphology (McCoy, 1987; Rogers, 2007). Rogers (2007) proposes a
209 method that accounts for the temperature sensitivity of the chemical reaction associated with
210 glass hydration. His method is built on the idea of estimating an *effective temperature*, which is
211 defined as the steady temperature needed to produce the same amount of hydration as observed
212 in a sample with a variable temperature history.

213 The effective temperature method requires a specification of the temperature sensitivity
214 of the process. The reaction rates for amino-acid racemization and glass hydration are known to
215 follow an Arrhenius relationship. Gillooly et al. (2001; 2002) and Brown et al. (2004), along
216 with others, have investigated the rates of a wide variety of biological processes, including
217 metabolic rate and growth rate, across a wide range of organisms, including fish. Their universal
218 metabolic equation is

219
$$B \propto M^{3/4} e^{-E_a/RT}, \quad (1)$$

220 where B is metabolic rate (kJ s^{-1}), M is body mass (kg), E_a is the activation energy (kJ mol^{-1}), R
221 is Boltzmann's constant ($8.314 \text{ kJ mol}^{-1} \text{ K}^{-1}$), and T is the absolute temperature (K). The
222 Arrhenius relationship for reaction rate as a function of temperature is accounted for by the
223 exponential factor on the right (Boltzman factor). Brown et al. (2004) recommended an average
224 value for $E_a = 0.63 \text{ eV} = 61 \text{ kJ/mol}$. They argue that this value holds for all organisms.

225 Ecological theory requires that growth rate be proportional to metabolic rate. The
226 equation above shows that warmer temperatures result in faster growth. Thus, our samples will
227 be biased towards the warmer times in their life cycle. The calculation of an effective
228 temperature removes this bias. Because there is little variation in body mass among adult gars,

229 growth rate for adult gars can be viewed as proportional to the Boltzman factor. As a result, the
 230 Rogers (2007) method for calculating effective temperature is directly applicable.

231 Following Rogers (2007), the time variation in temperature over a year is represented by

$$232 \quad T(t) = T_{MAT} + \frac{\Delta T_{SR}}{2} \sin(2\pi t) + \frac{\Delta T_{DR}}{2} \sin\left(\frac{2\pi t}{365}\right), \quad (2)$$

233 where T is temperature (K), t is time (a = annum), T_{MAT} is the mean annual temperature (K), and
 234 ΔT_{SR} and ΔT_{DR} are the seasonal and daily ranges in temperature (K). The mass production rate,
 235 P , (mass/time) of gar scales is represented by Arrhenius relationship,

$$236 \quad P = P_0 \exp\left(\frac{E_a}{RT}\right), \quad (3)$$

237 where P_0 is a pre-exponential constant. The effective temperature, T_e is defined by

$$238 \quad T_e = \int_0^1 P(T(t))T(t)dt / \int_0^1 P(T(t))dt, \quad (4)$$

239 which represents the weighted mean of the temperature, with the weighting provided by P . There
 240 is no analytical solution for (4), but the integrations are easily solved numerically (for details, see
 241 Rogers, 2007).

242 Figure 2 shows a comparison of $T_{\text{effective}}$ against T_{MAT} for 19,874 North America stations
 243 (excluding Greenland) for the time interval from 1900 to 2018 (surface air temperature at 2 m
 244 height above ground provided by the Global Historical Climatology Network (GHCN) database
 245 Menne et al. (2012)). These data were used to calculate mean values for T_{AM} , ΔT_{SR} , and ΔT_{DR} at
 246 each station. The stations provided an average record length of 11 years for these estimates due
 247 to partial records. Note that T_e is always greater than T_{MAT} by as much as 12 °C. This difference
 248 increases with decreasing temperature, which is consistent with the fact that surface air
 249 temperature is most steady in the tropics and most variable in the polar regions, and the
 250 production rate P increases with increasing temperature.

251 For our gar calibration, T_{AM} , ΔT_{SR} , and ΔT_{DR} were estimated for each sample site using
252 the 1-km gridded Daymet dataset (Thornton et al., 2017; Thornton et al., 1997). Daymet was
253 constructed using a truncated Gaussian filter to approximately 11,000 stations under the National
254 Weather Service Cooperative Observer Program (NWS COOP), weighting stations by distance
255 from an arbitrary point. Predicted temperatures were estimated using a weighted least-squares
256 regression. We added 1 °C to Daymet temperatures to account for the positive offset of river
257 water temperature relative to air temperature (Fricke and Wing, 2004).

258

259 2.3 Specimen pretreatment

260 Approximately 5 cm x 5 cm sections of scales were taken from the left lateral side of the
261 fish, as the alternative side is commonly left for archival purposes, and given to dermestid
262 beetles for several days to remove collagen and other organic tissues (Hefti et al., 1980).
263 Debrided scales were further cleaned by scalpel and tweezers. Approximately 1 g of scales from
264 each specimen were cryogenically milled in a 6750 Freezer/Mill (SPEX CertiPrep) for 3
265 minutes.

266 Unlike the bioapatite used in Wacker et al. (2016) and Eagle et al. (2010), gar scales have
267 an initial higher concentration of organic matter. We sampled whole scales, including the enamel
268 layer and the underlying bone, as it is difficult to distinguish between the two with the naked eye.
269 Both are assumed to have the same initial isotopic composition. The mineralized bone is
270 interwoven with collagen, and the enamel is covered by collagen during life. They are pitted with
271 vertical canals that contain miniature blood vessels and mesoderm cells (Kerr, 1952). Gar scales
272 interlock and are further connected *in vivo* by the fibrous collagen of the stratum compactum
273 (Gemballa and Bartsch, 2002). Gar scales share the same XRD peaks as carbonate

274 hydroxyapatite (LeGeros and Suga, 1980; LeGeros et al., 1967) but have high initial contents of
275 $9.4 \pm 0.8\%$ organic carbon and 3.24 ± 0.3 nitrogen (Supplemental Table 1), which is related to
276 the organic material that these scales possess *in vivo*.

277 Some of the organic material can be mechanically removed, but chemical treatment of
278 samples was needed for complete removal. Any stray hydroxyl groups on the collagen matrix,
279 such as from glycine, proline, and hydroxyproline (Eastoe, 1957) which surround the ganoine
280 scales, likely react with the acid during digestion, producing water, as detected by elevated mass
281 18 values. For a detailed discussion of the effect of chemical treatment methods on gar scale
282 clumped isotopic values, see Gray (2018).

283 Koch et al. (1997) found that treatment with 30% H_2O_2 did not affect the isotopic values
284 of enamel hydroxyapatite. Milled samples were sonicated (Sonicor DSC-100TH) for several
285 hours with 30% H_2O_2 to remove organic carbon. Scales were considered clean when bubbling
286 from the reaction ceased. Scales were then rinsed with DI water, agitated, and centrifuged; this
287 process was repeated six times. Samples were dried in a vacuum (Isotemp Vacuum Oven Model
288 280A, Fisher Scientific, USA) at 40 °C for two days. XRD showed an increase in bioapatite
289 peaks after sonication, particularly at the [002] and [211] peaks, 25.9° and $31.8^\circ 2\theta$,
290 respectively.

291

292 *2.4 Acid digestion and Δ_{47} Measurement*

293 Wacker et al. (2013) noted a sample size effect on Δ_{47} when carbonate samples <7 mg
294 were digested at 25 °C. Wacker et al. (2016) found a similar effect for bioapatite from elephant
295 tooth enamel. They inferred that at the lower reaction temperature, there was partial re-
296 equilibration of the resultant gas with water. Wacker et al. (2016) increased the reaction

297 temperature to 110 °C for bioapatite to decrease the reaction time. They noted that the partial
298 pressure of the water vapor above the acid was four times greater, which is much larger than
299 expected for a 20 °C increase in temperature. Water is known to adversely affect bond ordering
300 in CO₂ samples. Our choice of a 90 °C instead of a 25 °C reaction temperature was meant to
301 avoid this problem. It is also more consistent with the reaction temperature used in most clumped
302 isotope labs.

303 Samples ranging from 45 to 55 mg were reacted in an isolated McCrea vessel with 105%
304 H₃PO₄ ($\rho = 1.93 \text{ g/cm}^3$) at 90 °C. Reactions lasted for 20 to 40 minutes and were considered
305 complete when visible bubbles stopped forming. Because modern material has a large organic
306 component and the -OH⁻ group from the bioapatite scale reacts with the H⁺ ions in the acid to
307 form water, extra care was taken to purify the extracted CO₂ on a Pyrex vacuum line. For every
308 torr of CO₂ produced from the acid digestion, about 1 to 1.5 torr of water was also produced. To
309 avert re-equilibration with water, samples were kept under constant vacuum throughout the
310 reaction and were continuously collected. Water was removed by forcing the sample twice
311 through an ethanol-liquid nitrogen trap held at less than -85 °C. Sample CO₂ was then passed
312 through silver wool to remove any sulfur compounds (Eiler, 2007).

313 Purified CO₂ was then passed through a homemade stainless-steel column (1.22 m long x
314 0.3175 cm OD) filled with Poropak Q 50-80 mesh (Waters Technologies Co., USA) and housed
315 in a gas chromatograph (Varian CP-3800, USA). This step was to ensure that sample CO₂ had no
316 remaining hydrocarbons or halocarbon contaminants, which can interfere with the mass 47
317 measurement (Eiler and Schauble, 2004). The Poropak Q was ultimately chosen over Supelco Q-
318 Plot due to its better ability to handle organic rich samples.

319 During chromatography, samples were held at a constant -20 °C and carried with helium
320 at a rate of 5 mL/min for approximately 45 minutes through the column. CO₂ was frozen
321 cryogenically after being forced through the GC column and passed through the water trap two
322 more times before being placed on the mass spectrometer. The GC column was baked at 150 °C
323 between each sample run. After every four samples, or once daily, it was baked at 220 °C for 600
324 minutes (Huntington et al., 2009).

325 Measurements were performed on a MAT 253 dual-inlet gas-source isotope ratio mass
326 spectrometer (ThermoFisher Scientific, USA) housed at the Yale University Analytical and
327 Stable Isotope Center. The MAT 253 was modified to measure masses 44 through 49
328 simultaneously in dual-inlet mode, alternating between sample gas and reference gas. The
329 standard three Faraday cups were used to measure masses 44, 45, and 46, with an additional
330 three cups to measure masses 47, 48, and 49, with the same currents and resistances as Eiler and
331 Schauble (2004). Further modifications were made to the Yale mass spectrometer to allow
332 measurement of small samples (Zaarur et al., 2011). Measurement routines were as outlined by
333 Huntington et al. (2009) and Zaarur et al. (2011): nine acquisitions of 10 cycles each with eight
334 seconds of integration time for the reference and sample gas each cycle. There were two
335 additional acquisitions of two cycles each to measure the background voltage. Bulk oxygen and
336 carbon isotopic compositions were made using Oztech Trading Co. CO₂ (Safford, AZ) as a
337 working standard, with a composition of $\delta^{18}\text{O} = -3.629 \text{ ‰}$ and $\delta^{13}\text{C} = 24.992 \text{ ‰}$, which allowed
338 for conversion to the VSMOW scale.

339 Measurements of Δ_{47} were calculated based on the excess of mass 47 from a stochastic
340 distribution of isotopologues with varying bulk carbon and oxygen isotopic compositions. The
341 stochastic distribution was determined by heating pure CO₂, with a wide range of $\delta^{18}\text{O}$ and $\delta^{13}\text{C}$

342 compositions, to 1000 °C for two hours to reset its Δ_{47} value (Eiler and Schauble, 2004). These
343 heated gases were run on a weekly basis, or about every 10 to 15 samples. To correct for scale
344 compression, which varies with time in a single lab and between labs, CO₂ was equilibrated with
345 water at 25 °C (Affek, 2013; Dennis et al., 2011). Carrara marble was regularly run as an internal
346 carbonate standard, as well as cylinder CO₂ (Airgas, USA).

347 To fit data into an absolute reference frame (Dennis et al., 2011), data were adjusted
348 using an empirical transfer function slope that averages changes in the heated gas line over time.
349 Prior clumped isotope work had used ¹⁷O abundance correction values from Gonfiantini et al.
350 (1995), but their recommended λ of 0.5164 – the relationship between $\delta^{17}\text{O}$ and $\delta^{18}\text{O}$ – was
351 based on a study that used a combination of waters and rocks to estimate the coefficient
352 (Matsuhisa et al., 1978). Brand et al. (2010) recommended $\lambda = 0.528$ as a better representation of
353 the terrestrial fractionation of surface waters. Additionally, the choice of this λ value, along with
354 the R^{17} and R^{18} values as reported in Brand et al. (2010), appear to make Δ_{47} measurements truly
355 independent of the bulk isotopic composition (Daëron et al., 2016). Raw Δ_{47} were converted
356 using the Brand et al. (2010) parameters as outlined in Daëron et al. (2016).

357

358 **3. Results**

359 *3.1 Temperature dependence of Δ_{47} and independence from bulk composition*

360 The lack of correlation between the clumped isotopic measurement (Δ_{47}) and the isotopic
361 bulk composition ($\delta^{18}\text{O}_{\text{carbonate}}$ and $\delta^{13}\text{C}_{\text{carbonate}}$, hereafter labeled $\delta^{18}\text{O}_c$ and $\delta^{13}\text{C}$) suggested that
362 they were independent (Figures 3 and 4). $\delta^{13}\text{C}$ was assumed to be mostly influenced by diet. The
363 range of $\delta^{13}\text{C}$ values was consistent with the fact that gars are predators, or secondary consumers
364 (Fricke and Pearson, 2008; Gu et al., 1996). In addition, factors other than temperature and

365 $\delta^{18}\text{O}_{\text{water}}$ may influence the $\delta^{18}\text{O}_{\text{c}}$ – temperature relationship in modern fishes, such as the
366 specific placement of the carbonate ion in the bioapatite lattice (Kolodny and Luz, 1991).

367 The lowest Δ_{47} values obtained from gar scales were 0.657 to 0.664‰ from *A. tropicus*
368 specimens from Mexico, and the highest Δ_{47} values were 0.718 to 0.810‰ from *L. osseus*
369 specimens from Michigan, USA. A least squares linear regression of the inverse squared
370 effective temperature experienced by gars versus Δ_{47} values produced a calibration line

$$371 \quad \Delta_{47} = (0.1095 \pm 0.0159) \times 10^6 / T^2 - (0.5941 \pm 0.0548), \quad (5)$$

372 with $R^2 = 0.7358$ (Figure 5).

373 A second calibration line was calculated that included elephant tooth enamel as a high
374 temperature endmember ($T = 36.2 \text{ }^\circ\text{C}$; $\Delta_{47} = 0.582\text{‰}$; temperature from Kinahan et al. (2007)).
375 Sand tiger shark dentine was not added because its bulk isotopic composition is different from its
376 overlying enameloid (Löffler et al., 2019). The fluoride-rich quality of shark bioapatite sets it
377 apart from the other sampled species in the bioapatite calibration. The enameloid of the
378 Greenland shark (Löffler et al., 2019; Wacker et al., 2016) was not included because its growth
379 temperature was not well constrained. These sharks migrate from higher latitudes with
380 temperatures $\sim -2 \text{ }^\circ\text{C}$ to lower latitudes with water temperatures as warm as $10 \text{ }^\circ\text{C}$ (MacNeil et
381 al., 2012), and they are found from just below the surface to $>1200 \text{ m}$ depths (Yano et al., 2007).
382 The Greenland shark of Wacker et al. (2016) and Löffler et al. (2019) was recovered off of the
383 coast of Iceland, which is at the crossroads of several major currents with different salinities,
384 temperatures, and oxygen isotopic compositions. Temperatures of $7.0 \text{ }^\circ\text{C}$ are obtained when the
385 appropriate phosphate-oxygen thermometer (Puc at et al., 2010) is used to estimate its
386 temperature. Additionally, the effective temperature of a Greenland shark that on average

387 experiences temperatures of 2 °C is 4 °C; for 5 °C, it is 7 °C. The bioapatite from Eagle et al.
388 (2010) were not included as they correct ¹⁷O with the Gonfiantini et al. (1995) λ .

389 The combined calibration of T vs Δ_{47} for bioapatite from gars *in vivo* and for endotherms
390 that produce true enamel, with known internal body temperature, produce the calibration

$$391 \quad \Delta_{47} = (0.0987 \pm 0.0140) \times 10^6/T^2 - (0.4658 \pm 0.0481) \quad (6)$$

392 with $R^2 = 0.798$ (Figure 6).

393 The Δ_{47} values from gar scales are skewed high compared to the synthetic apatite of
394 Löffler et al. (2019). Equation (6) for all bioapatite is more robust due to its $X^2 = 1.410$ versus X^2
395 $= 2.790$ for the calibration from gar scales alone in Equation (5). A clear offset is recognized at
396 colder temperatures (<15 °C MAT).

397

398 **4. Discussion**

399 *4.1. Comparison to other calibrations*

400 The clumped isotope community is often troubled by the lack of consistency among lab
401 calibrations, but recent modifications to their development have helped minimize these
402 discrepancies. This was first addressed in Dennis et al. (2011), who developed an absolute
403 reference frame established on the projection of Δ_{47} measurements onto an “absolute scale”
404 based on theoretical predictions about the equilibrium relationship of Δ_{47} as a function of
405 temperature (Wang et al., 2004). The absolute reference frame provides support for inter-
406 laboratory reproducibility to a level of 0.017 and 0.008‰ (1 σ). The heated gas intercept was
407 also recalibrated to account for the scrambling (the fragmentation and recombination reactions of
408 the sample CO₂) within the ion source of a mass spectrometer.

409 There remains some discordance between labs, which some have attributed to differences
410 in the reaction temperature used for the phosphoric-acid step. It is well known that there is a
411 temperature-dependent isotopic fraction of CO₂ gas produced by phosphoric-acid dissolution of
412 carbonate. The acid fractionation factor between reactions at 25 °C and 90 °C was re-measured
413 by Henkes et al. (2013) as 0.076‰ ± 0.007‰, which is within 1 σ error to the original value.

414 Kelson et al. (2017) set to create a universal calibration using different methods of
415 synthesizing carbonates over a wide range of temperatures and added these results to the current
416 pool of Δ₄₇ measurements. The scatter between calibrations decreases with the use of the Brand
417 et al. (2010) parameters (Kelson et al., 2017).

418 A clumped isotope calibration using unvarying isotopically very heavy or very light bulk
419 composition carbonate with the Gonfiantini et al. (1995) parameter may be noticeably different
420 from a calibration that does not. Zaarur et al. (2013) created isotopically very light δ¹³C
421 carbonate—from -35.09‰ to -17.53‰—compared to other synthetic calibrations. Holding the
422 acid digestion temperature constant, it has a steeper slope, even after correction with Brand et al.
423 (2010). Kelson et al. (2017) explains the main calibration discrepancy as perhaps arising from
424 lab differences in isolating the CO₂ before isotopic measurement. Lab standards were
425 reproducible among the setup used by Zaarur et al. (2013) and others, so this is likely not the
426 cause (Dennis et al., 2011; Henkes et al., 2013). It may be biased because the starting bulk
427 composition of the synthetic carbonate is lighter from that used in other labs, as they are
428 generally -20 ‰ or heavier. It likely does not fall on the terrestrial meteoric water line.

429 When the samples in this study were modified using the ¹⁷O correction parameters of
430 Brand et al. (2010) as exemplified in Daëron et al. (2016), the slope was not affected, only the
431 intercept, in similar fashion to other ¹⁷O corrected synthetic carbonate calibrations (Kelson et al.,

432 2017). If the bulk composition truly affects the calibration due to the choice of ^{17}O parameters,
433 the range of $\delta^{13}\text{C}$ from this study, from -5.29‰ to -9.47‰, should have minimal effects, since
434 they are not on either extreme: isotopically very enriched or very depleted.

435 The laboratory set-up used here with a GC column of Poropak Q and constant CO_2
436 entrapment during the reaction is similar to several labs, but it does not account for the
437 significantly steeper slope seen in bioapatite. Additionally, the in-house standard YCM was run
438 at 25 °C and 90 °C through a Supelco Q-Plot column and through a Poropak Q column within a
439 GC. No significant difference was seen in Δ_{47} among the disparate cleaning methods. Only the
440 acid digestion temperature had an effect, which was expected. The in-house clumped isotope
441 standard, Yale Carrara Marble (YCM), has a long-term running average of $\Delta_{47\text{abs}} = 0.418 \pm 0.016$
442 (1σ) at 25 °C. At 90 °C, $\Delta_{47\text{abs}} = 0.357 \pm 0.015$ (1σ), an offset within error to the acid
443 fractionation factor $\alpha_{25-90} = 1.0076 \pm 0.007$ (Henkes et al., 2013).

444

445 *4.2 Biological explanations for discrepancy*

446 The enamel scales of gar are produced by proteins encoded by the genes *ambn* and *enam*,
447 which are also present in lobe-finned vertebrates, including mammals (Braasch et al., 2016).
448 When carbonate is incorporated into bioapatite, it either takes the place of hydroxyl (A-type
449 substitution) or phosphate (B-type substitution), with the latter placement 28% more prevalent in
450 mammalian bone (Rey et al., 1989).

451 The fractionation factor between inorganic phosphate (and consequently carbonate) and
452 bioapatite in mammals is species dependent or at least affected by a combination of genetic and
453 lifestyle influences (Ayliffe and Chivas, 1990; D'Angela and Longinelli, 1990; Longinelli, 1984).
454 Gar likely follow a calibration curve similar to mammals, but a mammalian-only calibration

455 curve is not feasible because mammals maintain a constant 37 °C body temperature regardless of
456 phylogenetic placement.

457 The potential of isotopic mixing as postulated by Henkes et al. (2013) for mollusks
458 should not apply for gar; the mollusks were time averaged over a year, whereas these fish are
459 averaged over several years to decades. Even if isotopic mixing affected the calibration curve,
460 Henkes et al. (2013) estimated that the effect it would have on the mollusk curve would be
461 minimal.

462 Incorporation of carbon from dissolved inorganic carbon (DIC) from dietary sources has
463 been observed in shark teeth (Vennemann et al., 2001). This DIC has a residual low Δ_{47} signal
464 when incorporated into body tissues, which only becomes an issue if the DIC was diffused from
465 the environment. The one correlation that may indicate kinetic isotope effects, $\delta^{18}\text{O}_{\text{carbonate}}$, shows
466 no relationship to Δ_{47} . No enrichment in measured $\delta^{18}\text{O}_{\text{carbonate}}$ over expected values is seen for
467 samples. There is also no correlation between Δ_{47} and $\delta^{13}\text{C}$ (Figure 4 B).

468

469 *4.3 Benefits of natural calibrations*

470 Laboratory experiments can only partially recreate complex isotopic systems. Watkins et
471 al. (2014) found that non-equilibrium isotopic effects from inorganic calcite precipitation can
472 produce up to a 2‰ $\delta^{18}\text{O}$ offset. The universal calibration of Kelson et al. (2017) may be true for
473 inorganic calcite, but there are other confounding variables, especially those affiliated with
474 biogenic mineral precipitation (e.g., Henkes et al., 2013; Saenger et al., 2012; Thiagaraian et al.,
475 2011; Zaarur et al., 2011). Hidden variables due to biology or other factors are accounted for
476 when using a natural calibration on natural samples. In this regard, the Δ_{47} of bioapatite samples,
477 including fossils, should not be converted to temperature using a purely carbonate calibration.

478

479 **5. Conclusions**

480 The clumped isotopic composition of bioapatite from multiple sources, including gar
481 scales, produces a real temperature signal that is different from the Δ_{47} -T relationship for
482 carbonates, most notably at low temperatures. This divergence cannot be attributed to laboratory
483 differences or disparity in data transformation and therefore likely represents a unique
484 relationship possessed by vertebrates. Its steeper slope makes it more sensitive to temperature
485 changes, further increasing its utility on land.

486 Ganoine is found not only in gar scales but also in the scales of closely related species,
487 such as the living Polypteriformes and fossil Semionotiformes. Assuming a similar Δ_{47} -T
488 relationship occurs for these ancient fish, terrestrial temperatures could be estimated as far back
489 as the Triassic. Today, gar are commonly seen as ‘trash fish,’ as they can inhabit low-quality
490 water and their tough exterior makes them largely inedible. This fundamental survivorship
491 quality, along with paleontologists’ relative apathy toward them, gives gar and their affiliated
492 isolated scales great potential to reconstruct past terrestrial climates.

493 Furthermore, the independent temperature proxy, Δ_{47} , can be coupled with $\delta^{18}\text{O}_{\text{carbonate}}$
494 from the same single clumped isotope measurement to infer $\delta^{18}\text{O}_{\text{water}}$. The $\delta^{18}\text{O}_{\text{carbonate}}$ value
495 could be replaced with one from $\delta^{18}\text{O}_{\text{phosphate}}$, as it provides a more robust signal. The $\delta^{18}\text{O}_{\text{water}}$
496 values from a single measurement offer insight into the hydrological cycle. When applied to
497 fossil samples from terrestrial paleoenvironments across a region or across time, these values can
498 indicate changes in the cycle.

499 Gar scales are abundant in the fossil record. Two of the most concentrated localities
500 where gar scales are found are the Green River Formation of Wyoming and the Messel

501 Formation in Germany (Grande, 2010), both of which formed during the Eocene period. While
502 the greatest concentrations of gar fossils are from North America and Europe, there are also
503 notable fossil deposits from the Cretaceous of Morocco and Brazil. All of these deposits are
504 inferred to be fluvial or lacustrine in origin and represent glimpses into terrestrial environments.

505

506 **Acknowledgements**

507 This research was partially funded through a Yale Institute for Biospheric Studies grant
508 to K.E. Gray. Deepest gratitude goes to the late Mark Pagani for his ideas and insight into this
509 project. All measurements were done at the Yale Analytical and Stable Isotope Center (YASIC).
510 Greg Watkins-Colwell of the Yale Peabody Museum assisted in gar scale removal and cleaning.
511 Douglas Nelson, Fishes Collection Manager at the Museum of Zoology at the University of
512 Michigan greatly assisted in providing specimens to sample. Other acquired specimens were
513 obtained with help of the Mississippi Department of Wildlife, Fisheries, and Parks; the
514 Tennessee Wildlife Resources Agency; and the Illinois Department of Natural Resources.

515

516 **References**

517 Affek, H.P. (2013) Clumped Isotope Equilibrium and the Rate of Isotope Exchange Between CO₂ and Water.
518 *American Journal of Science* 313, 309-325.
519 Affek, H.P. and Eiler, J.M. (2006) Abundance of mass-47 of CO₂ in urban air, car exhaust, and human breath.
520 *Geochimica et Cosmochimica Acta* 70, 1-12.
521 Ayliffe, L.K. and Chivas, A.R. (1990) Oxygen isotope composition of bone phosphate of Australian kangaroos:
522 Potential as a paleoenvironmental recorder. *Geochimica et Cosmochimica Acta* 54, 2603-2609.
523 Bohn, S., Kreiser, B.R. and Bodine, K.A. (2017) Natural Hybridization of Lepisosteids: Implications for Managing
524 the Alligator Gar. *North American Journal of Fisheries Management* 37, 405-413.
525 Boyde, A. (1964) *The Structure and Development of Mammalian Enamel*, Department of Anatomy. University of
526 London, London.
527 Braasch, I., Gehrke, A.R., Smith, J.J., Kawasaki, K., Manousaki, T., Pasquier, J., Amores, A., Desvignes, T., Batzel,
528 P., Catchen, J., Berlin, A.M., Campbell, M.S., Barrell, D., Martin, K.J., Mulley, J.F., Ravi, V., Lee, A.P.,
529 Nakamura, T., Chalopin, D., Fan, S., Weisel, D., Cañestro, C., Sydes, J., Beaudry, F.E.G., Sun, Y., Hertel,
530 J., Beam, M.J., Fasold, M., Ishiyama, M., Johnson, J., Kehr, S., Lara, M., Letaw, J.H., Litman, G.W.,
531 Litman, R.T., Mikami, M., Ota, T., Saha, N.R., Williams, L., Stadler, P.F., Wang, H., Taylor, J.S.,
532 Fontenot, Q., Ferrara, A., Searle, S.M.J., Aken, B., Yandell, M., Schneider, I., Yoder, J.A., Volff, J.-N.,
533 Meyer, A., Amemiya, C.T., Venkatesh, B., Holland, P.W.H., Guiguen, Y., Bobe, J., Shubin, N.H., Di

534 Palma, F., Alföldi, J., Lindblad-Toh, K. and Postlethwait, J.H. (2016) The spotted gar genome illuminates
535 vertebrate evolution and facilitates human-teleost comparisons. *Nature Genetics* 48, 427-437.

536 Brand, W.A., Assonov, S.S. and Coplen, T.B. (2010) Correction for the ^{17}O interference in $d(^{13}\text{C})$ measurements
537 when analyzing CO_2 with stable isotope mass spectrometry (IUPAC Technical Report). *Pure Appl. Chem.*
538 82, 1719-1733.

539 Bromage, T.G. (1991) Enamel incremental periodicity in the Pig-Tailed Macaque: A Polychrome Fluorescent
540 Labeling Study of Dental Hard Tissues. *American Journal of Physical Anthropology* 86, 205-214.

541 Brown, J.H., Gillooly, J.F., Allen, A.P., Savage, V.M. and West, G.B. (2004) Toward a metabolic theory of ecology.
542 *Ecology* 85, 1771-1789.

543 Buckmeier, D.L. (2008) Life History and Status of Alligator Gar *Atractosteus spatula*, with Recommendations for
544 Management, in: TPWD Inland Fisheries Report, H.o.t.H.F.S.C. (Ed.).

545 Buckmeier, D.L., Smith, N.G. and Daugherty, D.J. (2013) Alligator Gar Movement and Microhabitat Use in the
546 Lower Trinity River, Texas. *Transactions of the American Fisheries Society* 142, 1025-1035.

547 Buckmeier, D.L., Smith, N.G. and Reeves, K.S. (2012) Utility of Alligator Gar Age Estimates from Otoliths,
548 Pectoral Fin Rays, and Scales. *Transactions of the American Fisheries Society* 141, 1510-1519.

549 Came, R.E., Eiler, J.M., Veizer, J., Azmy, K., Brand, U. and Weidman, C.R. (2007) Coupling of surface
550 temperatures and atmospheric CO_2 concentrations during the Paleozoic era. *Nature* 449, 198-201.

551 D'Angela, D. and Longinelli, A. (1990) Oxygen isotopes in living mammal's bone phosphate: Further results.
552 *Chemical Geology* 86, 75-82.

553 Daëron, M., Blamart, D., Peral, M. and Affek, H. (2016) Absolute isotopic abundance ratios and the accuracy of Δ_{47}
554 measurements. *Chemical Geology* 441, 83-96.

555 Dean, M.C. (1987) Growth layers and incremental markings in hard tissues; a review of the literature and some
556 preliminary observations about enamel structure in *Paranthropus boisei*. *Journal of Human Evolution* 16,
557 157-172.

558 Dennis, K.J., Affek, H.P., Passey, B.H., Schrag, D.P. and Eiler, J.M. (2011) Defining an absolute reference frame
559 for 'clumped' isotope studies of CO_2 . *Geochimica et Cosmochimica Acta* 75, 7117-7131.

560 Eagle, R.A., Schauble, E.A., Tripathi, A.K., Tütken, T., Hulbert, R.C. and Eiler, J.M. (2010) Body temperatures of
561 modern and extinct vertebrates from ^{13}C - ^{18}O bond abundances in bioapatite. *Proceedings of the National*
562 *Academy of Science* 107, 10377-10382.

563 Eastoe, J.E. (1957) The Amino Acid Composition of Fish Collagen and Gelatin. *Biochemical Journal* 65, 363-368.

564 Eiler, J.M. (2007) "Clumped-isotope" geochemistry - the study of naturally-occurring, multiply-substituted
565 isotopologues. *Earth and Planetary Science Letters* 262, 309-327.

566 Eiler, J.M. and Schauble, E.A. (2004) $^{18}\text{O}^{13}\text{C}^{16}\text{O}$ in Earth's atmosphere. *Geochimica et Cosmochimica Acta* 68,
567 4767-4777.

568 Ferrara, A.M. (2001) Life history strategy of Lepisosteidae: Implications for the conservation and management of
569 Alligator gar, Fisheries and Allied Aquacultures. Auburn University, Auburn, Alabama, p. 145.

570 Fricke, H.C., Clyde, W.C., O'Neil, J.R. and Gingerich, P. (1998) Evidence for rapid climate change in North
571 America during the latest Paleocene thermal maximum: oxygen isotope compositions of biogenic
572 phosphate from the Bighorn Basin (Wyoming). *Earth and Planetary Science Letters* 160, 193-208.

573 Fricke, H.C. and Pearson, D.A. (2008) Stable isotope evidence for changes in dietary niche partitioning among
574 hadrosaurian and ceratopsian dinosaurs of the Hell Creek Formation, North Dakota. *Paleobiology* 34, 534-
575 552.

576 Fricke, H.C. and Wing, S.L. (2004) Oxygen isotope and paleobotanical estimates of temperature and $\delta^{18}\text{O}$ latitude
577 gradients over North American in Eocene. *American Journal of Science* 304, 612-635.

578 Gemballa, S. and Bartsch, P. (2002) Architecture of the integument in lower Teleostomes: functional morphology
579 and evolutionary implications. *Journal of Morphology* 253, 290-309.

580 Germeraad, J.H., Hopping, C.A. and Muller, J. (1968) Palynology of Tertiary Sediments from Tropical Areas.
581 *Review of Palaeobotany and Palynology* 6, 189 - 348.

582 Ghosh, P., Adkins, J., Affek, H.P., Balta, B., Guo, W., Schauble, E.A., Schrag, D. and Eiler, J.M. (2006a) ^{13}C - ^{18}O
583 bonds in carbonate minerals: A new kind of paleothermometer. *Geochimica et Cosmochimica Acta* 70,
584 1439-1456.

585 Ghosh, P., Eiler, J., Campana, S.E. and Feeney, R.F. (2007) Calibration of the carbonate 'clumped isotope'
586 paleothermometer for otoliths. *Geochimica et Cosmochimica Acta* 71, 2736-2744.

587 Ghosh, P., Garzzone, C.N. and Eiler, J.M. (2006b) Rapid Uplift of the Altiplano revealed through ^{13}C - ^{18}O bonds in
588 paleosol carbonates. *Science* 311, 511-515.

589 Gillooly, J.F., Brown, J.H., West, G.B., Savage, V.M. and Charnov, E.L. (2001) Effects of Size and Temperature on
590 Metabolic Rate. *Science* 293, 2248-2251.

591 Gillooly, J.F., Charnov, E.L., West, G.B., Savage, V.M. and Brown, J.H. (2002) Effects of size and temperature on
592 developmental time. *Nature* 417, 70-73.

593 Gonfiantini, Stichler and Rozanski (1995) IAEA-TECDOC-825, International Atomic Energy Agency, Vienna, pp.
594 13-29.

595 Grande, L. (2010) An empirical synthetic pattern study of gars (*Lepisosteiformes*) and closely related species, based
596 mostly on skeletal anatomy. The resurrection of *Holostei*. *American Society of Ichthyologists and*
597 *Herpetologists*.

598 Gray, K. (2018) Reconstructing Terrestrial Clumped Isotope Thermometry and Phosphate Oxygen
599 Isotopes from Gar Scales, *Geology and Geophysics*. Yale University, New Haven, CT, p. 158.

600 Grimes, S.T., Matthey, D.P., Hooker, J.J. and Collinson, M.E. (2003) Paleogene paleoclimate reconstruction using
601 oxygen isotopes from land and freshwater organisms: the use of multiple proxies. *Geochimica et*
602 *Cosmochimica Acta* 67, 4033-4047.

603 Grossman, E.L. and Ku, T.-L. (1986) Oxygen and carbon isotope fractionation in biogenic aragonite: temperature
604 effects. *Chemical Geology* 59, 59-74.

605 Gu, B., Schelske, C.L. and Hoyer, M.V. (1996) Stable isotopes of carbon and nitrogen as indicators of diet and
606 tropic structure of the fish community in a shallow hypereutrophic lake. *Journal of Fish Biology* 49, 1233-
607 1243.

608 Haase, B.L. (1969) An ecological life history of the longnose gar, *Lepisosteus osseus* (Linnaeus), in Lake Mendota
609 and in several other lakes of southern Wisconsin, *Zoology*. University of Wisconsin, p. 225.

610 Hefti, E., Trechsel, U., Rüfenacht, H. and Fleisch, H. (1980) Use of dermestid beetles for cleaning bones. *Calcified*
611 *Tissue International* 31, 45-47.

612 Henkes, G.A., Passey, B.H., Wanamaker Jr., A.D., Grossman, E.L., Ambrose Jr., W.G. and Carroll, M.L. (2013)
613 Carbonate clumped isotope compositions of modern marine mollusk and brachiopod shells. *Geochimica et*
614 *Cosmochimica Acta* 106, 307-325.

615 Huntington, K.W., Eiler, J.M., Affek, H.P., Guo, W., Bonifacie, M., Yeung, L.Y., Thiagarajan, N., Passey, B.H.,
616 Tripathi, A.K., Daëron, M. and Came, R. (2009) Methods and limitations of 'clumped' CO₂ isotope (Δ_{47})
617 analysis by gas-source isotope ratio mass spectrometry. *Journal of Mass Spectrometry* 44, 1318-1329.

618 Inoue, J.G., Miya, M., Venkatesh, B. and Nishida, M. (2005) The mitochondrial genome of Indonesian coelacanth
619 *Latimeria mendadoensis* (Sarcopterygii: Coelanthiformes) and divergence time estimation between the two
620 coelacanths. *Gene* 349, 227-235.

621 Johnson, B.L. and Noltie, D.B. (1997) Demography, growth, and reproductive allocation in stream-spawning
622 Longnose gar. *Transactions of the American Fisheries Society* 126, 438-466.

623 Kelson, J.R., Huntington, K.W., Schauer, A.J., Saenger, C. and Lecher, A.R. (2017) Toward a universal carbonate
624 clumped isotope calibration: Diverse synthesis and preparatory methods suggest a single temperature
625 relationship. *Geochimica et Cosmochimica Acta* 197, 104-131.

626 Kerr, T. (1952) The scales of primitive living actinopterygians. *Proceedings of the Zoological Society of London*
627 122.

628 Kinahan, A.A., Inge-moller, R., Bateman, P.W., Kotze, A. and Scantlebury, M. (2007) Body temperature daily
629 rhythm adaptations in African savanna elephants (*Loxodonta africana*). *Physiology & Behavior* 92, 560-
630 565.

631 Koch, P.L., Tuross, N. and Fogel, M. (1997) The Effects of Sample Treatment and Diagenesis on the Isotopic
632 Integrity of Carbonate in Biogenic Hydroxylapatite. *Journal of Archaeological Science* 24, 417-429.

633 Kolodny, Y. and Luz, B. (1991) Oxygen isotopes in phosphates of fossil fish - Devonian to Recent, in: H.P. Taylor,
634 H.P., O'Neil, J.R., Kaplan, I.R. (Eds.), *Stable Isotope Geochemistry: A Tribute to Samuel Epstein*.
635 *Geochemical Society Special Publications*, pp. 105-119.

636 Lee, D.S., Gilbert, C.R., Hocutt, C.H., Jenkins, R.E., McAllister, D.E. and Stauffer, J., Jay R. (1980) Atlas of North
637 American freshwater fishes. North Carolina State Museum of Natural Sciences, Raleigh, NC.

638 LeGeros, R.Z. and Suga, S. (1980) Crystallographic Nature of Fluoride in Enameloids of Fish. *Calcified Tissue*
639 *International* 32, 169-174.

640 LeGeros, R.Z., Trautz, O.R., LeGeros, J.P., Klein, E. and Shirra, W.P. (1967) Apatite Crystallites: Effects of
641 Carbonate on Morphology. *Science* 155, 1409-1411.

642 Leng, M.J. and Marshall, J.D. (2004) Palaeoclimate interpretation of stable isotope data from lake sediment
643 archives. *Quaternary Science Reviews* 23, 811-831.

644 Löffler, N., Fiebig, J., Mulch, A., Tütken, T., Schmidt, B.C., Bajnai, D., Conrad, A.C., Wacker, U. and Böttcher,
645 M.E. (2019) Refining the temperature dependence of the oxygen and clumped isotopic compositions of
646 structurally bound carbonate in apatite. *Geochimica et Cosmochimica Acta* 253, 19-38.

647 Longinelli, A. (1984) Oxygen isotopes in mammal bone phosphate: A new tool for paleohydrological and
648 paleoclimatological research? *Geochimica et Cosmochimica Acta* 48, 385-390.

649 MacNeil, M.A., MacMeans, B.C., Hussey, N.E., Vecsei, P., Svavarsson, J., Kovacs, K.M., Lydersen, C., Treble,
650 M.A., Skomal, G.B., Ramsey, M. and Fisk, A.T. (2012) Biology of the Greenland Shark *Somniosus*
651 *microcephalus*. *Journal of Fish Biology* 80, 991-1018.

652 Markwick, P.J. (1998) Fossil crocodylians as indicators of Late Cretaceous and Cenozoic climates: implications for
653 using palaeontological data in reconstructing palaeoclimate. *Palaeogeography, Palaeoclimatology,*
654 *Palaeoecology* 137, 205-271.

655 Matsuhisa, Y., Goldsmith, J.R. and Clayton, R.N. (1978) Mechanisms of hydrothermal crystallization of quartz at
656 250 °C and 15 kbar. *Geochimica et Cosmochimica Acta* 42, 173-182.

657 McCoy, W.D. (1987) The precision of amino acid geochronology and paleothermometry. *Quaternary Science*
658 *Reviews* 6, 43-54.

659 McGrath, P. (2010) The Life History of Longnose Gar, *Lepisosteus osseus*, an Apex Predator in the Tidal Waters of
660 Virginia, School of Marine Science. The College of William and Mary, p. 177.

661 Menne, M.J., Durre, I., Vose, R.S., Gleason, B.E. and Houston, T.G. (2012) An overview of the Global Historical
662 Climatology Network-Daily Database. *Journal of Atmospheric and Oceanic Technology* 29, 897-910.

663 Netsch, N. and Witt, A. (1962) Contributions to the Life History of the Longnose Gar, (*Lepisosteus osseus*) in
664 Missouri. *Transactions of the American Fisheries Society* 91, 251-262.

665 Pearson, A. and Ingalls, A.E. (2013) Assessing the use of archaeal lipids as marine environmental proxies. *Annual*
666 *Review of Earth and Planetary Science* 41, 359-384.

667 Peterse, F., van der Meer, J., Schouten, S., Weijers, J.W.H., Fierer, N., Jackson, R.B., Kim, J.-H. and Damsté, S.J.S.
668 (2012) Revised calibration of the MBT-CBT paleotemperature proxy based on branched tetraether
669 membrane lipids in surface soils. *Geochimica et Cosmochimica Acta* 96, 215-229.

670 Prokhorov, I., Kluge, T. and Janssen, C. (2019) Optical clumped isotope thermometry of carbon dioxide. *Scientific*
671 *Reports* 9.

672 Pucéat, E., Joachimski, M.M., Bouilloux, A., Monna, F., Bonin, A., Motreuil, S., Morinière, P., Hénard, S., Mourin,
673 J., Dera, G. and Quesne, D. (2010) Revised phosphate–water fractionation equation reassessing
674 paleotemperatures derived from biogenic apatite. *Earth and Planetary Science Letters* 298, 135-142.

675 Rey, C., Collins, B., Goehl, T., Dickson, I.R. and Glimcher, M.J. (1989) The Carbonate Environment in Bone
676 Mineral: A Resolution-Enhanced Fourier Transform Infrared Spectroscopy Study. *Calcified Tissue*
677 *International* 45, 157-164.

678 Rogers, A.K. (2007) Effective hydration temperature of obsidian: a diffusion theory analysis of time-dependent
679 hydration rates. *Journal of Archaeological Science* 34, 656-665.

680 Saenger, C., Affek, H.P., Felis, T., Thiagarajan, N., Lough, J.M. and Holcomb, M. (2012) Carbonate clumped
681 isotope variability in shallow water corals: Temperature dependence and growth-related vital effects.
682 *Geochimica et Cosmochimica Acta* 99, 224-242.

683 Schauble, E.A., Ghosh, P. and Eiler, J. (2006) Preferential formation of ¹³C-¹⁸O bonds in carbonate minerals,
684 estimated using first-principles lattice dynamics. *Geochimica et Cosmochimica Acta* 70, 2510-2529.

685 Smylie, M., Shervette, V. and McDonough, C. (2016) Age, Growth, and Reproduction in Two Coastal Populations
686 of Longnose Gars. *Transactions of the American Fisheries Society* 145, 1.

687 Snedden, G.A., Kelso, W.E. and Rutherford, A.D. (1999) Diel and Seasonal Patterns of Spotted Gar Movement and
688 Habitat Use in the Lower Atchafalaya River Basin, Louisiana. *Transactions of the American Fisheries*
689 *Society* 128.

690 Solomon, D.R. (2012) Life history, growth, and genetic diversity of the spotted gar *Lepisosteus oculatus* from
691 peripheral and core populations, *Natural Resources and Environment*. University of Michigan, p. 171.

692 Still, C., Powell, R., Aubrecht, D., Kim, Y., Helliker, B., Roberts, D., Richardson, A.D. and Goulden, M. (2019)
693 Thermal imaging in plant and ecosystem ecology: applications and challenges. *Ecosphere* 10.

694 Swart, P.K. (2015) The geochemistry of carbonate diagenesis: The past, present, and future. *Sedimentology* 62,
695 1233-1304.

696 Thiagarajan, N., Adkins, J. and Eiler, J. (2011) Carbonate clumped isotope thermometry of deep-sea corals and
697 implications for vital effects. *Geochimica et Cosmochimica Acta* 75, 4416-4425.

698 Thomson, K.S. and McCune, A.R. (1984) Scale Structure as Evidence of Growth Patterns in Fossil Semionotid
699 Fishes. *Journal of Vertebrate Paleontology* 4, 422-429.

- 700 Thornton, M.M., Thornton, P.E., Wei, Y., Vose, R.S. and Boyer, A.G. (2017) Daymet: Station-Level Inputs and
701 Model Predicted Values for North America, Version 3. ORNL DAAC, Oak Ridge, Tennessee, USA.
- 702 Thornton, P.E., Running, S.W. and White, M.A. (1997) Generating surfaces of daily meteorological variables over
703 large regions of complex terrain. *Journal of Hydrology* 190, 214-251.
- 704 Traverse, A. (2007) *Paleopalynology*, 2nd ed. Springer, Netherlands.
- 705 Tripathi, A.K., Eagle, R.A., Thiagarajan, N., Gagnon, A.C., Bauch, H., Halloran, P.R. and Eiler, J.M. (2010) ^{13}C - ^{18}O
706 isotope signatures and 'clumped isotope' thermometry in foraminifera and coccoliths. *Geochimica et*
707 *Cosmochimica Acta* 74, 5697-5717.
- 708 Vennemann, T.W., Hegner, E., Cliff, G. and Benz, G.W. (2001) Isotopic composition of recent shark teeth as a
709 proxy for environmental conditions. *Geochimica et Cosmochimica Acta* 65, 1583-1599.
- 710 Wacker, U., Fiebig, J. and Schoene, B.R. (2013) Clumped isotope analysis of carbonates: comparison of two
711 different acid digestion techniques. *Rapid Communications in Mass Spectrometry* 27, 1631-1642.
- 712 Wacker, U., Rutz, T., Löffler, N., Conrad, A.C., Tütken, T., Böttcher, M.E. and Fiebig, J. (2016) Clumped isotope
713 thermometry of carbonate-bearing apatite: Revised sample pre-treatment, acid digestion, and temperature
714 calibration. *Chemical Geology* 443, 97-110.
- 715 Wang, Z., Schauble, E.A. and Eiler, J.M. (2004) Equilibrium thermodynamics of multiply substituted isotopologues
716 of molecular gases. *Geochimica et Cosmochimica Acta* 68, 4779 - 4797.
- 717 Watkins, J.M., Hunt, J.D., Ryerson, F.J. and DePaolo, D.J. (2014) The influence of temperature, pH, and growth rate
718 on the d^{18}O composition of inorganically precipitated calcite. *Earth and Planetary Science Letters* 404,
719 332-343.
- 720 Wilf, P. (1997) When are leaves good thermometers? A new case for leaf margin analysis. *Paleobiology* 23, 373-
721 390.
- 722 Wing, S.L. and Greenwood, D.R. (1993) Fossils and Fossil Climate: The case for Equable Continental Interiors in
723 the Eocene. *Philosophical Transactions of the Royal Society B* 341, 243-252.
- 724 Wolfe, J.A. and Spicer, R.A. (1999) Fossil Leaf Character States: Multivariate Analysis, in: Jones, T.P., Rowe, N.P.
725 (Eds.), *Fossil Plants and Spores: Modern Techniques*. Geological Society, London, pp. 233-239.
- 726 Yano, K., Stevens, J.D. and Compagno, L.J.V. (2007) Distribution, reproduction, and feeding of the Greenland
727 shark *Somniosus (Somniosus) microcephalus*, with notes on two other sleeper sharks, *Somniosus*
728 *(Somniosus) pacificus* and *Somniosus (Somniosus) antarcticus*. *Journal of Fish Biology* 70, 374-390.
- 729 Zaarur, S., Affek, H.P. and Brandon, M.T. (2013) A revised calibration of the clumped isotope thermometer. *Earth*
730 *and Planetary Science Letters* 382, 47-57.
- 731 Zaarur, S., Olack, G. and Affek, H.P. (2011) Paleo-environmental implication of clumped isotopes in land snail
732 shells. *Geochimica et Cosmochimica Acta* 75, 6859-6869.

733

734

Locality	Coordinates	MAT (°C)	Effective T (°C)	Seasonal Temperatures (°C) (1 σ error)			<i>n</i>
				AMJ	MJJA	DJF	
Bay Port, MI, USA	43.8569° N, 83.3743° W	9.12 ± 0.22	11.4	14.31 ± 0.29	19.60 ± 0.28	-3.72 ± 0.52	3
North Scott Lake, MI, USA	42.3307° N, 85.9988° W	8.57 ± 0.17	12.9	13.53 ± 0.31	18.61 ± 0.28	-3.25 ± 0.48	2
Rend Lake Dam, IL, USA	38.0371° N, 88.9562° W	13.61 ± 0.19	17.2	19.31 ± 0.22	23.48 ± 0.21	1.67 ± 0.38	1
Ullin, IL, USA	37.2733° N, 89.1838° W	14.21 ± 0.21	16.4	19.10 ± 0.31	23.57 ± 0.32	2.50 ± 0.39	1
Estill Springs, TN, USA	35.2557° N, 86.1332° W	14.87 ± 0.15	17.2	19.43 ± 0.19	23.74 ± 0.22	4.09 ± 0.37	3
Yazoo City, MS, USA	32.8966° N, 90.5419° W	18.41 ± 0.21	20.1	22.78 ± 0.28	26.35 ± 0.29	8.78 ± 0.39	6
Silver Springs, FL, USA	29.1638° N, 82.0777° W	21.73 ± 0.16	22.3	24.33 ± 0.16	26.76 ± 0.08	15.47 ± 0.50	1
Villahermosa, Tabasco, MX	17.9970° N, 92.9280° W	24.81 ± 0.21	26.3	27.08 ± 0.26	27.09 ± 0.25	21.40 ± 0.37	1

Table 1. Seasonal and annual climatic data from NOAA’s National Centers for Environmental Information Climate Data Online and Mexico’s Servicio Meteorológico Nacional and are averaged for approximately 15 years before the collection date of the gar specimen. AMJ = April May June, MJJA = May June July August, DJF = December January February

Sample	Locality	$\delta^{18}\text{O}_{\text{water}}$	n	Species	$\delta^{18}\text{O}$ (‰ VPBD)	$\delta^{13}\text{C}$ (‰ VPBD)	Δ_{47} (Abs. Brand)	Δ_{47} SE
MDF 1	Yazoo City, Mississippi	-3.91	3	<i>L. osseus</i>	0.037	-9.357	0.674	0.008
MDF 2			4	<i>L. osseus</i>	1.224	-6.759	0.644	0.005
MDF 3			3	<i>L. osseus</i>	-0.009	-7.334	0.697	0.006
MDF 4			2	<i>L. osseus</i>	-1.993	-9.500	0.645	0.027
MDF 5			3	<i>L. osseus</i>	1.765	-7.890	0.673	0.011
MDF 6			3	<i>L. osseus</i>	0.666	-7.468	0.680	0.015
YPM 27686	Estill Springs, Tennessee	-5.68	4	<i>L. osseus</i>	-0.329	-5.966	0.674	0.007
YPM 27692			3	<i>L. osseus</i>	-0.494	-6.979	0.710	0.017
YPM 27693			3	<i>L. osseus</i>	0.133	-7.066	0.695	0.007
UMMZ 230705v1	North Scott Lake, Michigan	-7.94	3	<i>L. oculatus</i>	-3.581	-7.682	0.789	0.007
UMMZ 230705v2			2	<i>L. oculatus</i>	-5.178	-8.051	0.768	0.007
UMMZ 180463v1	Bay Port, Michigan	-9.37	3	<i>L. osseus</i>	-0.370	-5.981	0.754	0.015
UMMZ 180463v2			2	<i>L. osseus</i>	-6.606	-6.188	0.741	0.011
UMMZ 180463v3			2	<i>L. osseus</i>	-2.785	-5.329	0.764	0.046
YPM 27215	Rend Lake Dam, Illinois	-4.13	2	<i>L. osseus</i>	6.118	-7.716	0.687	0.0002
IX-03-01					Ullin, Illinois	-4.13	3	<i>L. osseus</i>
UMMZ 145166	Silver Springs, Florida	-0.84	3	<i>L. osseus</i>	-2.344	-11.311	0.668	0.013
UMMZ 145167			4	<i>L. osseus</i>	-1.944	-5.016	0.666	0.028
UMMZ 187727	Tabasco, Mexico	-2.64	3	<i>A. tropicus</i>	4.595	-6.768	0.661	0.002

Table 2. Data for all samples. Δ_{47} values are given in the absolute reference frame as outlined in Dennis et al. (2011). ^{17}O is corrected using the Brand et al. (2010) parameters. Abbreviations are YPM for the Yale Peabody Museum, UMMZ for the University of Michigan Museum of Zoology, and MDF for Mississippi Department of Wildlife, Fisheries, and Parks.

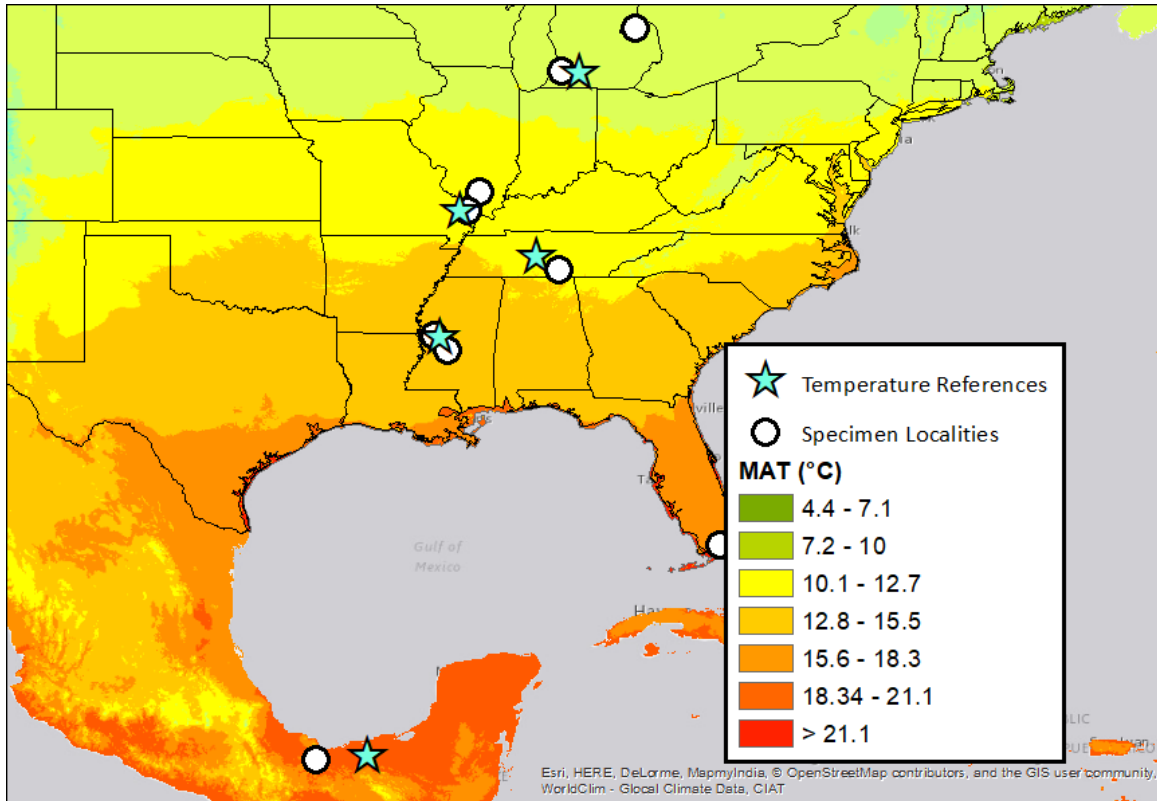


Figure 1. Map of specimen localities (white circles) and the closest weather station (light blue stars) for temperature data in table 1 (National Oceanic & Atmospheric Administration, National Environmental Satellite, Data, and Information Science) superimposed on MAT (WorldClim Global Climate Data). Although gars do not migrate, specimens were preferentially chosen from dams or reservoirs or small streams to minimize temperature fluctuations.

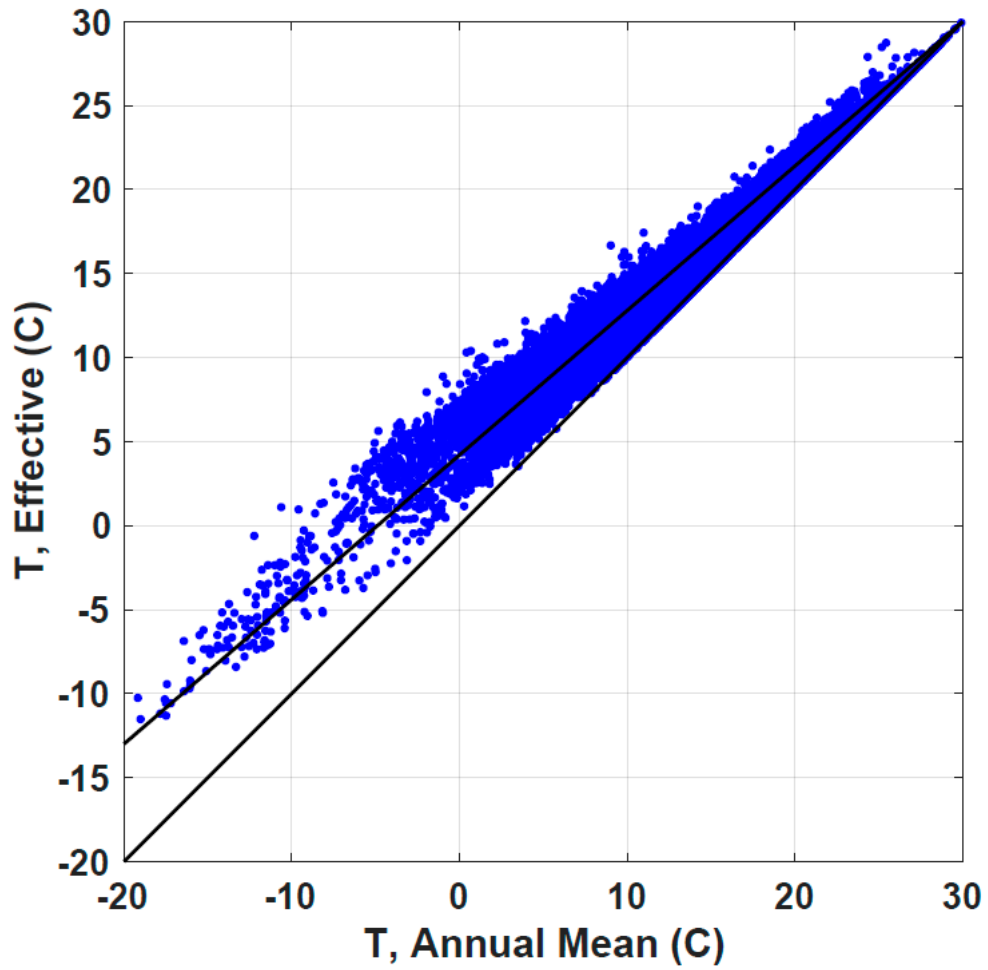


Figure 2. Comparison of $T_{\text{effective}}$ against MAT ($^{\circ}\text{C}$) for 19,874 North America stations (excluding Greenland) for the time interval from 1900 to 2018.

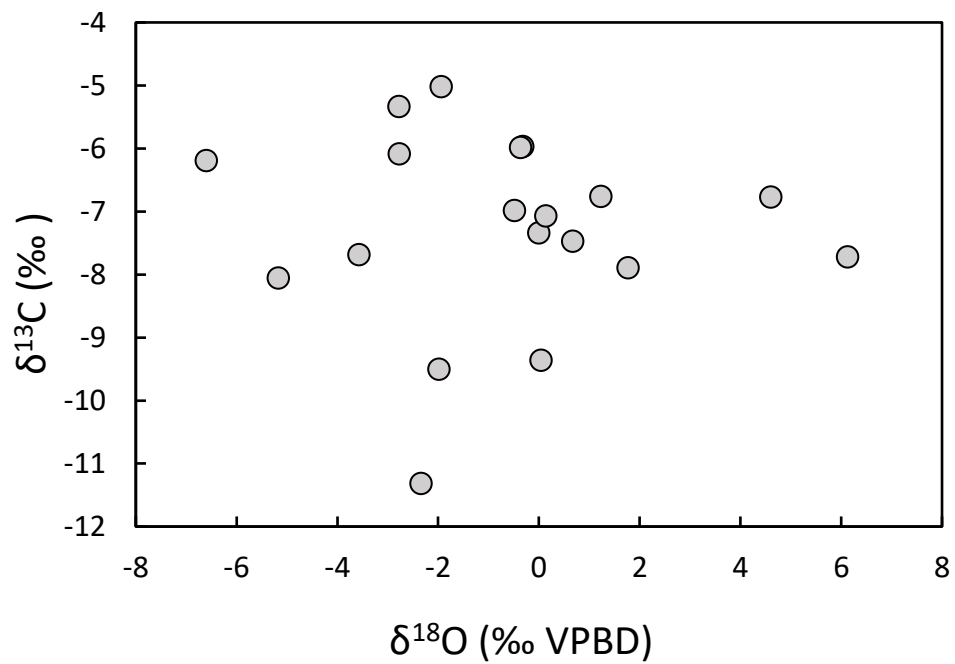


Figure 3. Comparison between $\delta^{18}\text{O}$ (VPBD) and $\delta^{13}\text{C}$. There is no correlation between $\delta^{18}\text{O}$ and $\delta^{13}\text{C}$.

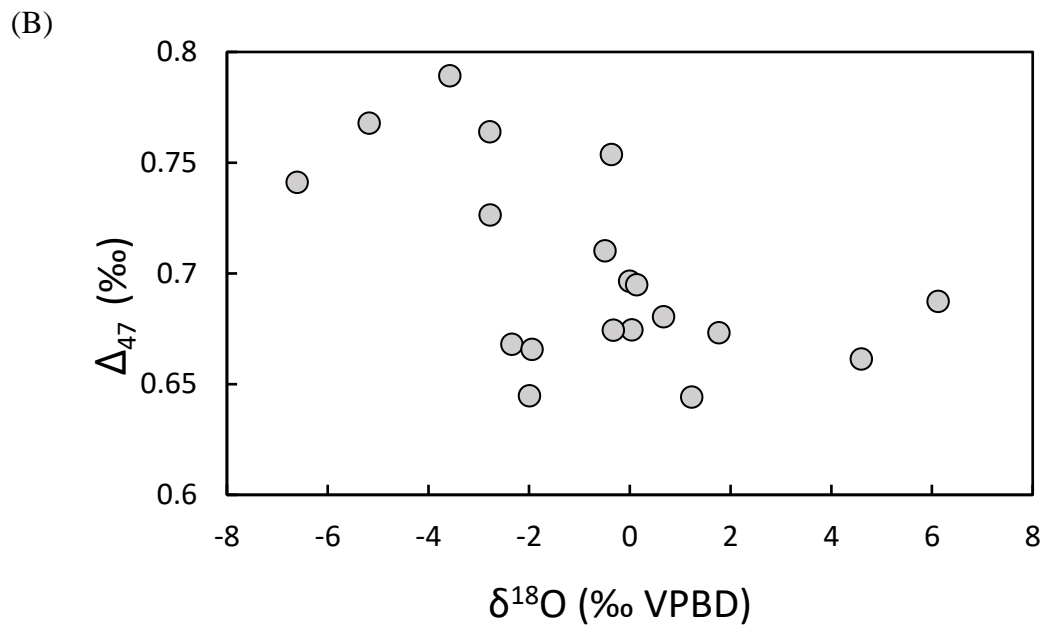
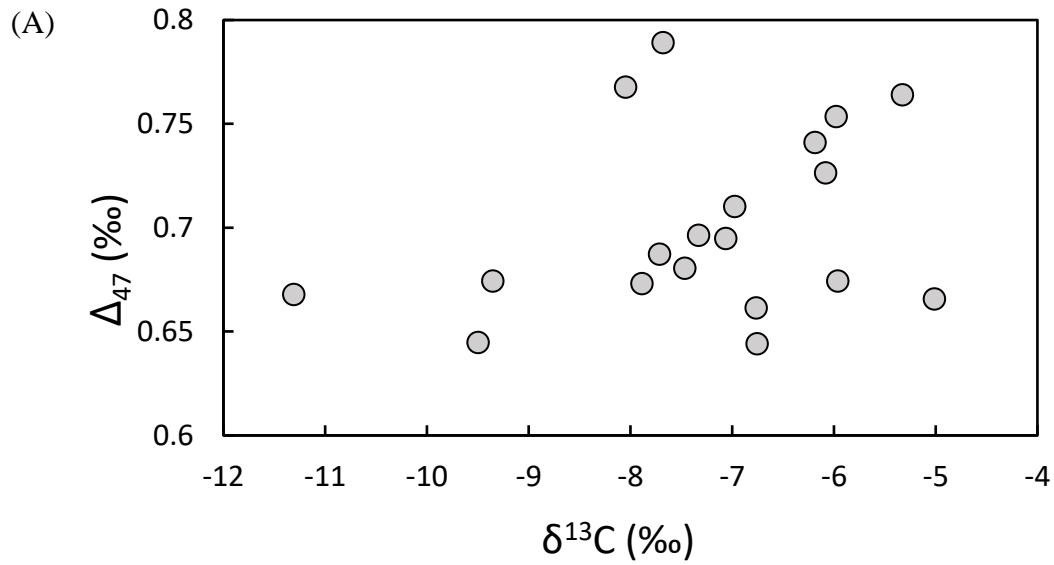


Figure 4. Comparison between Δ_{47} and $\delta^{13}\text{C}$ (A) and Δ_{47} and $\delta^{18}\text{O}$ (VPBD) in gar scales (B).

There is no correlation between $\delta^{18}\text{O}$ or $\delta^{13}\text{C}$ and Δ_{47} . Δ_{47} is independent of the bulk composition.

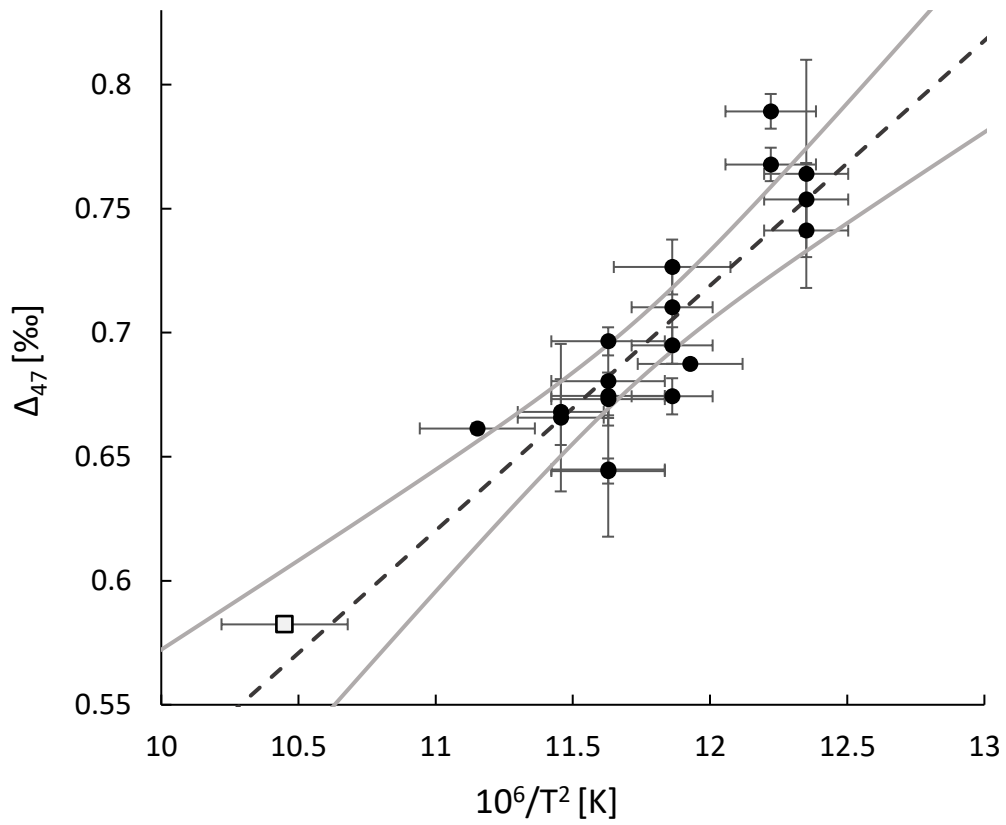


Figure 6. Empirical relationship between Δ_{47} in biogenic apatite, including gar scales, and temperature (K). White open circle is elephant enamel from Löffler et al. (2019).